Chemical Science

EDGE ARTICLE

View Article Online
View Journal | View Issue

Cite this: *Chem. Sci.*, 2017, **8**, 3164

High-level *ab initio* potential energy surface and dynamics of the $F^- + CH_3I$ S_N2 and proton-transfer reactions†

Balázs Olasz, István Szabó‡ and Gábor Czakó*

Received 4th January 2017
Accepted 15th February 2017

DOI: 10.1039/c7sc00033b

rsc.li/chemical-science

Bimolecular nucleophilic substitution (S_N2) and proton transfer are fundamental processes in chemistry and $F^- + CH_3I$ is an important prototype of these reactions. Here we develop the first full-dimensional *ab initio* analytical potential energy surface (PES) for the $F^- + CH_3I$ system using a permutationally invariant fit of high-level composite energies obtained with the combination of the explicitly-correlated CCSD(T)-F12b method, the aug-cc-pVTZ basis, core electron correlation effects, and a relativistic effective core potential for iodine. The PES accurately describes the S_N2 channel producing $I^- + CH_3F$ *via* Walden-inversion, front-side attack, and double-inversion pathways as well as the proton-transfer channel leading to $HF + CH_2I^-$. The relative energies of the stationary points on the PES agree well with the new explicitly-correlated all-electron CCSD(T)-F12b/QZ-quality benchmark values. Quasiclassical trajectory computations on the PES show that the proton transfer becomes significant at high collision energies and double-inversion as well as front-side attack trajectories can occur. The computed broad angular distributions and hot internal energy distributions indicate the dominance of indirect mechanisms at lower collision energies, which is confirmed by analyzing the integration time and leaving group velocity distributions. Comparison with available crossed-beam experiments shows usually good agreement.

Introduction

Bimolecular nucleophilic substitution (S_N2) is one of the best-known reaction classes in organic chemistry. The atomic-level description of the back-side attack inversion and front-side attack retention mechanisms of S_N2 reactions was already presented in the book of Ingold in 1953.[1] According to the simple picture of the $X^- + CH_3Y \rightarrow XCH_3 + Y^-$ [X, Y = F, Cl, Br, I] reactions, the back-side attack Walden-inversion pathway involves a C_{3v} ion–dipole pre-reaction complex ($X^-\cdots H_3CY$), a central transition state (TS) $(X\cdots H_3C\cdots Y)^-$, and a C_{3v} post-reaction complex ($XCH_3\cdots Y^-$), whereas the front-side attack pathway goes through a high-energy $(H_3CXY)^-$ TS, where X directly replaces Y without inversion. However, recent theoretical and experimental studies show that this simple picture is not complete and the dynamics of S_N2 reactions are much more complex.[2–8] Besides the above described direct pathways, indirect mechanisms play a key role in the dynamics. For the $Cl^- + CH_3I$ reaction a so-called roundabout mechanism[9] was found in 2008 and for the $F^- + CH_3Cl$ reaction simulations revealed a double-inversion[6] pathway in 2015, which was also identified in aqueous solution[10] in 2016. Furthermore, in the case of the F^- nucleophile a hydrogen-bonded pre-reaction complex ($F^-\cdots HCH_2Y$) was found to play an important role in the dynamics.[5,11] In the case of the $F^- + CH_3Y$ S_N2 reactions, where Y = Cl and I, a recent joint crossed-beam and trajectory study showed that the leaving group can also influence the dynamics, since the $F^- + CH_3Cl$ reaction was found to be significantly more direct than $F^- + CH_3I$.[7] This means that the direct rebound mechanism dominates in $F^- + CH_3Cl$, whereas slow indirect complex-forming pathways are more likely in the $F^- + CH_3I$ reaction.

The present study focuses on the $F^- + CH_3I$ reaction, which has been recently investigated both experimentally and theoretically.[11–14] Previous reaction dynamics simulations[11–13] of the title reaction have been restricted to the use of the direct dynamics approach due to the lack of an analytical potential energy surface (PES). Here, we report such a PES for the $F^- + CH_3I$ system, which allows efficient quasiclassical trajectory (QCT) computations and opens the door for future quantum dynamics studies. Utilizing the large number of trajectories

Department of Physical Chemistry and Materials Science, Institute of Chemistry, University of Szeged, Rerrich Béla tér 1, Szeged H-6720, Hungary. E-mail: gczako@chem.u-szeged.hu

† Electronic supplementary information (ESI) available: Benchmark classical and adiabatic relative energies (Table S1), vibrational frequencies of all the stationary points (Tables S2 and S3), direct/indirect trajectory separation function parameters (Table S4), entrance-channel potential (Fig. S1), structures of the minima and saddle points corresponding to the abstraction channel (Fig. S2), reaction probabilities (Fig. S3), trajectory integration time distributions (Fig. S4), trajectory integration time *vs.* I^- velocity distributions (Fig. S5), and mechanism-specific reaction probabilities (Fig. S6). See DOI: 10.1039/c7sc00033b

‡ Present address: Department of Chemistry, King's College London, London SE1 1DB, UK.

obtained on the PES, we can compute statistically robust integral and differential cross sections as well as product internal energy distributions allowing quantitative comparisons with previous crossed-beam experiments.[11,12,14] We can also determine whether double-inversion trajectories can occur in the F^- + CH_3I reaction, which have never been seen before in this system even if smaller double-inversion barrier height was recently predicted[15] for F^- + CH_3I than that of F^- + CH_3Cl. Furthermore, besides the S_N2 pathways, a proton transfer between the reactants can also occur. The present study aims to simulate both the S_N2 and proton-transfer channels using the newly developed global PES.

Methods

The PES is represented by fitting high-level *ab initio* energies using the permutationally invariant polynomial approach.[16–20] Roughly 50 000 energy points are computed at the explicitly-correlated CCSD(T)-F12b/aug-cc-pVTZ level of theory[21,22] using a relativistic effective core potential and the corresponding aug-cc-pVTZ-PP basis set[23] for iodine. Core correlation effects, which can be important for the heavy iodine, are also considered as an additive correction obtained as difference between all-electron and frozen-core energies at the CCSD(T)/aug-cc-pwCVDZ-PP level of theory. The PES is fitted using a 5th order polynomial expansion of Morse-type variables, $\exp(-r_{ij}/a)$, where r_{ij} denotes inter-atomic distances and a = 3 bohr. Note that in many previous studies considering, for example, reactions of atoms with methane, an a value of 2 bohr was used.[24] However, in the case of S_N2 reactions, where long-range ion–dipole interactions present, a larger a value, *i.e.*, more diffuse fitting basis, is needed. After several test fits with different a values, we have chosen a = 3 bohr, which provides a good description at large distances as shown in Fig. S1 of the ESI.† The number of the linear fitting parameters is 3313, which are determined by a weighted least-squares fit, where each energy, E that is relative to the global minimum, has a weight of $E_0/(E + E_0)$, where E_0 is 0.1 in atomic units. Weights are used to suppress the high-energy data, which are out of the range of chemical importance. Our previous studies[5,6] on F^- + CH_3Cl used E_0 = 0.05 a.u.; here a larger E_0 is chosen, because F^- + CH_3I is more exothermic than F^- + CH_3Cl.

The new PES accurately describes the S_N2 channel *via* the above-mentioned different reaction pathways as well as the proton-transfer channel leading to HF + CH_2I^-. The energy diagram of the complex PES is shown in Fig. 1, where the relative energies obtained from the PES are compared to high-level benchmark *ab initio* data. The most important structural parameters of the stationary points obtained at CCSD(T)-F12b with aug-cc-pVDZ-PP and aug-cc-pVTZ-PP basis sets as well as from the PES are shown in Fig. 2 and S2† for the S_N2 and abstraction channels, respectively. The benchmark classical relative energies of the stationary points are computed using a composite method based on CCSD(T)-F12b/aug-cc-pVQZ-PP energies and CCSD(T)/aug-cc-pwCVTZ-PP core correlation corrections at CCSD(T)-F12b/aug-cc-pVTZ-PP geometries (Table S1†). The best adiabatic relative energies are determined by adding a harmonic zero-point energy (ZPE) correction, obtained at the CCSD(T)-F12b/aug-cc-pVTZ-PP level of theory, to the classical energies. The CCSD(T)-F12b/aug-cc-pVnZ-PP (n = D and T) and PES harmonic vibrational frequencies of all the stationary points are given in Tables S2 and S3.† All the

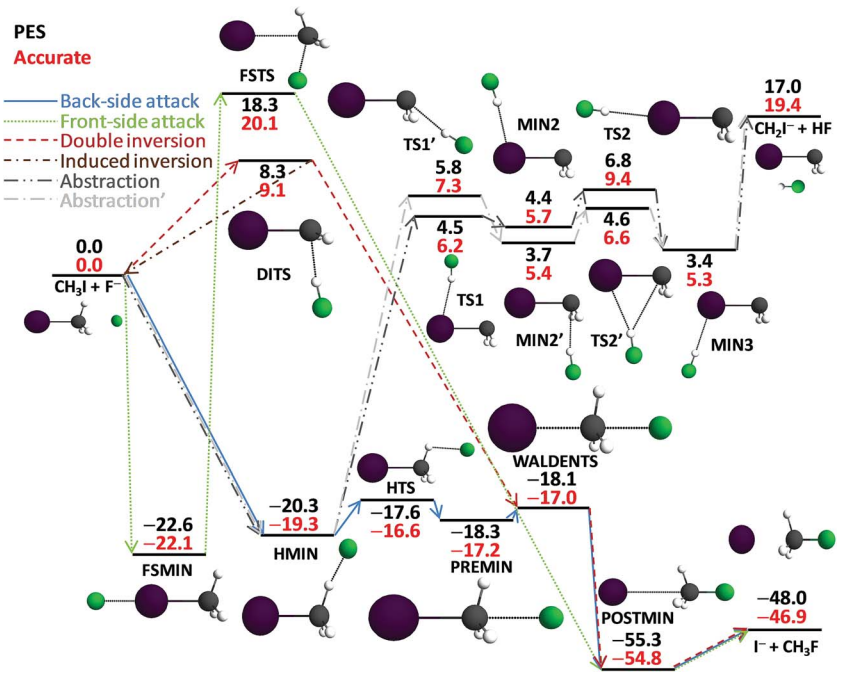

Fig. 1 Potential energy surface of the F^- + CH_3I S_N2 and proton-abstraction reactions showing the classical relative energies (kcal mol^{-1}) of the stationary points obtained from the analytical PES and by an accurate explicitly-correlated composite *ab initio* method.

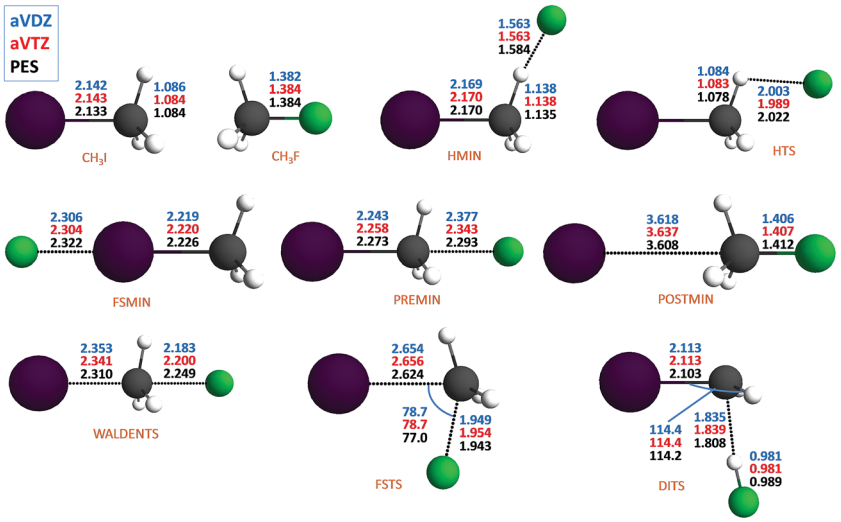

Fig. 2 Stationary-point structures corresponding to the S_N2 channel of the $F^- + CH_3I$ reaction showing the representative structural parameters (distances in Å and angles in degrees) obtained at CCSD(T)-F12b/aug-cc-pVDZ-PP (aVDZ) and CCSD(T)-F12b/aug-cc-pVTZ-PP (aVTZ) as well as by using the analytical potential energy surface (PES).

electronic structure computations are performed with the Molpro package.[25]

QCT computations are carried out for the $F^- + CH_3I$ ($v = 0$) reaction on the new analytical PES using standard normal-mode sampling[26] to prepare the initial vibrational ground state ($v = 0$) of CH_3I. Trajectories are run at collision energies (E_{coll}) of 1.0, 4.0, 7.4, 10.0, 15.9, 35.3, and 50.0 kcal mol^{-1} using a time step of 0.0726 fs. The impact parameters, b, are scanned from 0 to b_{max} with a step size of 0.5 bohr and 5000 trajectories are computed at each b. The b_{max} values are found to be 30, 20, 17, 15, 13, 10, and 9 bohr for the above collision energies, respectively. Note that b_{max} values are determined by running trajectories at increasing fixed b values using a step of 0.5 bohr until the reaction probability becomes 0. The final cross sections are obtained by a b-weighted numerical integration of the reaction probabilities over impact parameters from 0 to b_{max}. This approach is different from that which generates non-uniform b values between 0 and b_{max} using a Monte Carlo sampling, where the accurate value of b_{max} is important.[27–29] Of course, the two approaches converge to the same results with increasing number of trajectories and decreasing b steps for the former method. The impact parameter dependence of the reaction probabilities for both the S_N2 and abstraction channels at all the above collision energies are shown in the ESI (Fig. S3†). The present study considers more than 1 million trajectories. The maximum number of time steps for each trajectory is 5 million (363 ps), but the direct trajectories are only about 0.5–2 ps long and most of the trajectories finish within ~30 ps (for more details see Fig. S4†). The average CPU time of a trajectory is between 8 and 200 s strongly depending on the collision energy, impact parameter, and computer hardware. Note that the analytical potential ensures that the computation of forces during the trajectory propagation has almost no cost compared to direct dynamics simulations at the same level of theory.

Results and discussion

As shown in Table S1,† the CCSD(T)-F12b energies with aug-cc-pVDZ-PP and aug-cc-pVTZ-PP bases agree within about 0.2 kcal mol^{-1}, the core correlation effects have positive signs and are in the range of 0.0–0.8 kcal mol^{-1}, and the ZPE corrections are ranging from −3.5 to +2.0 kcal mol^{-1} for all the stationary points shown in Fig. 1. Thus, the ZPE corrections can be significant, since they decrease the exothermicity of the S_N2 channel by 1.8 kcal mol^{-1} and decrease the endothermicity of the abstraction channel by 3.5 kcal mol^{-1}. For the Walden-inversion TS the ZPE effect is negligible, whereas the ZPE correction decreases the abstraction as well as double-inversion barriers by about 2 kcal mol^{-1}. As shown in Fig. 1, the PES reproduces the high-level benchmark energies with 1 kcal mol^{-1} accuracy for the S_N2 pathways and somewhat larger differences of about 2 kcal mol^{-1} are seen for the abstraction channel. It is important to note that Zhang, Xie, and Hase[13] recently reported the same stationary points for the abstraction channel using B97-1/ECP/d/aug-cc-pVDZ level of theory, which usually overestimate the present benchmark values by 0.7 kcal mol^{-1} on average (the maximum deviation is 1.2 kcal mol^{-1} for TS1′ using our notation). Thus, our high-level energies confirm the reliability of the B97-1/ECP/d method for direct dynamics studies of the title reaction, at least at not too high energies.

Utilizing the benchmark classical relative energies we can characterize the different reaction pathways of the $F^- + CH_3I$ reaction. The S_N2 reaction is highly exothermic (−46.9 kcal mol^{-1}) with a submerged Walden-inversion TS (−17.0, relative to the reactant asymptote), a double-inversion barrier (9.1 kcal mol^{-1}), and a much higher front-side attack barrier (20.1 kcal mol^{-1}). The proton-abstraction channel is endothermic (19.4 kcal mol^{-1}) with several minima and saddle points above the reactants by about 5–10 kcal mol^{-1}, but well below the HF + CH_2I^- products. It is important to emphasize that the energy

level of the proton-abstraction products is significantly above the double-inversion TS and slightly below the front-side attack TS, similar to the F^- + CH_3Cl reaction, where the double-inversion pathway was discovered.[6] Thus, one can expect double-inversion trajectories below the threshold energy of the abstraction and front-side attack S_N2 pathways. In the entrance channel of the F^- + CH_3I reaction we have found several stationary points. Besides the C_{3v} ion–dipole complex (−17.2 kcal mol^{-1}), there is a hydrogen-bonded C_s complex (−19.3 kcal mol^{-1}) which corresponds to a significantly deeper minimum than the C_{3v} complex. The two minima is separated by a TS (−16.6 kcal mol^{-1}) above the C_s and C_{3v} minima by 2.7 and 0.6 kcal mol^{-1}, respectively. Furthermore, a front-side $F^-\cdots ICH_3$ C_{3v} complex (−22.1 kcal mol^{-1}), where F^- is connected to the I atom, also exits in the entrance channel. This complex may play a significant role in the dynamics, because the $F^-\cdots ICH_3$ minimum is deeper by 4.9 and 2.8 kcal mol^{-1} than the above-mentioned back-side C_{3v} and hydrogen-bonded minima, respectively.

As seen in Fig. 2 and S2 and Tables S2 and S3,† the PES reproduces the benchmark bond lengths and angles as well as the vibrational frequencies with reasonable accuracy. Here we just emphasize a few points. Even if the Walden-inversion barrier of S_N2 reactions is usually called "central", in the present case, the C–I distance is only stretched by 0.2 Å relative to the corresponding equilibrium distance in the reactant molecule, whereas the C–F distance is 0.8 Å longer than that in the product molecule. Thus, for the F^- + CH_3I reaction we can say that the Walden inversion has an early barrier (reactant-like TS), in accord with the Hammond postulate[30] for an exothermic reaction. At the double-inversion TS the H–F distance is stretched by 0.06 Å relative to the bond length of the HF molecule, whereas at the proton-abstraction minima and saddle points the corresponding effects are only around 0.02 Å. Furthermore, the intermolecular H$\cdots$C distance at the double-inversion TS is 1.8 Å, that is much shorter than the corresponding distances of 2.1–2.2 Å at the similar abstraction stationary points. Among the TSs the double-inversion, the front-side attack, and the Walden-inversion saddle points have the largest imaginary frequencies that are 767i, 591i, and 231i, in cm^{-1}, respectively, at the CCSD(T)-F12b/aug-cc-pVTZ-PP level, in good agreement with the corresponding PES values of 775i, 582i, and 206i. Note that the large imaginary frequency of the double-inversion saddle point makes this TS different from the abstraction TSs, which have imaginary frequencies around 100i. Thus, on one hand, there are several properties of the double-inversion TS which separate it from the abstraction TSs. On the other hand, as pointed out by Zhang, Xie, and Hase,[13] intrinsic reaction coordinate (IRC) computations show that the double-inversion TS is connected to the proton-transfer TSs. However, trajectories may not follow the IRC reaction path; therefore, the investigation of the role of the TSs in the double-inversion dynamics of the title reaction is an important future research direction.

Fig. 3 shows the cross sections as a function of collision energy for the different reaction pathways of the title reaction. The S_N2 cross sections are extremely large at low E_{coll} and

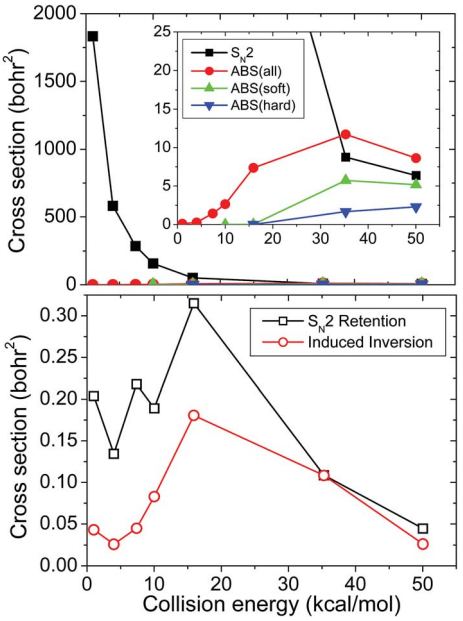

Fig. 3 Cross sections as a function of collision energy for the S_N2, abstraction, S_N2 retention (front-side attack + double inversion), and induced-inversion pathways of the F^- + CH_3I reaction. For the abstraction (ABS) channel results are shown without (all), with soft (discarding trajectories if the sum of the product vibrational energies is less than the sum of ZPEs), and with hard (discarding trajectories if either product violates ZPE) ZPE constraints.

sharply decrease as E_{coll} increases, as expected for a highly exothermic barrierless reaction. Applying ZPE constraint, the abstraction channel opens around E_{coll} = 15 kcal mol^{-1} in accord with its endothermicity of 15.9 kcal mol^{-1}. Without ZPE constraint, the abstraction cross sections are significantly larger and do not have a threshold. We consider both soft and hard ZPE constraints. The soft constraint discards trajectories if the sum of the product vibrational energies is less than the sum of ZPEs (obtained in the harmonic approximation), whereas the hard constraint discards trajectories if either HF or CH_2I^- has less vibrational energy than the corresponding ZPE. Note that a sophisticated alternative of treating the ZPE issue is the use of the one-dimensional Gaussian binning (1GB) method,[31–33] but this technique cannot provide realistic absolute cross sections due to the normalization issue, therefore we rely on the simpler soft and hard ZPE constraints. The soft and hard ZPE constraints give similar, physically correct thresholds, but the hard cross sections are substantially smaller as shown in Fig. 3. Recently, Zhang, Xie, and Hase[13] reported cross sections of 30.7 ± 7.9 and 7.5 ± 2.9 bohr^2 for the S_N2 and abstraction channels, respectively, obtained from a DFT/B91-1 direct dynamics computation at E_{coll} = 35.3 kcal mol^{-1}. When they applied ZPE constraint for the CH_2I^- product, the abstraction cross section became 5.4 ± 1.4 bohr^2. Our PES gives substantially smaller cross section (8.8 bohr^2) for the S_N2 channel, which, however, agrees better with an MP2 direct dynamics result of 6.4 ± 1.1 bohr^2.[34] For the abstraction, the present cross section of 11.7 bohr^2 without ZPE constraint is in reasonable agreement with the DFT/B91-1 result of 7.5 ± 2.9 bohr^2. Furthermore, our soft

constrained cross section (5.7 bohr^2) agrees well with the above-cited CH_2I^- constrained value of 5.4 ± 1.4 bohr^2. Note that the error bars of the direct dynamics results reflect the statistical uncertainty of the simulation, which is negligible in our case. The uncertainty due to the inaccuracy of the on-the-fly or analytical PES is hardly predictable, but obviously large especially for the S_N2 channel where the B97-1/ECP/d/aug-cc-pVDZ level and the present PES seem to deviate significantly, at least at high energies. The branching ratio between the S_N2 and proton-abstraction channels was recently measured by Wester and co-workers.[14] In the E_{coll} range of 30–50 kcal mol^{-1} the abstraction channel was found to contribute about 20% to the total reactivity. Without ZPE constraint the present simulation overestimates the abstraction cross sections and gives about 60% contribution. Nevertheless, using the hard ZPE constraint the abstraction cross sections drop to around 20% of the total cross section, in good agreement with experiment. This indicates that the use of the ZPE constraint can be important to get realistic results from a QCT simulation.

Configuration-retaining S_N2 cross sections are also shown in Fig. 3. These retention cross sections are about two orders of magnitude smaller than the inversion ones. Examination of many retention trajectories indicates that at low E_{coll} all of the retention trajectories occur *via* the double-inversion mechanism, whereas at collision energies above 20 kcal mol^{-1} the front-side attack pathway also opens. Double inversion is usually a slow indirect process, whereas the front-side attack is fast and direct. However, we found that one cannot distinguish between the two mechanisms based on simply the integration time, as we did in the case of the $F^- + CH_3Cl$, $F^- + CH_3F$, and $F^- + CHD_2Cl$ reactions.[6,35,36] Fig. 3 also shows the cross sections for the induced inversions of the CH_3I reactant, which are not followed by a substitution resulting in an inverted reactant. The E_{coll} dependence of the induced and double inversions is similar, both have a maximum at E_{coll} = 20 kcal mol^{-1}. At low E_{coll} the probability of induced inversion is smaller than that of the double inversion, showing that the first inversion is usually followed by a second inversion. Due to the fact that the adiabatic double-inversion barrier height of the $F^- + CH_3I$ reaction (7.0 kcal mol^{-1}) is significantly smaller than that of the $F^- + CH_3Cl$ reaction (14.0 kcal mol^{-1}),[6] we predicted[15] that the double inversion could be more likely in the $F^- + CH_3I$ system. The present QCT results support this, since the double-inversion cross sections can be as high as 0.3 bohr^2 for $F^- + CH_3I$, whereas the corresponding value is only 0.05 bohr^2 for $F^- + CH_3Cl$.[6] Furthermore, the maximum of the double-inversion cross sections, that is at E_{coll} = 30 kcal mol^{-1} for $F^- + CH_3Cl$, is at a smaller E_{coll} of 20 kcal mol^{-1} for $F^- + CH_3I$.

Comparison of the computed and measured[12] differential cross sections as well as product internal energy distributions of the S_N2 channel is shown in Fig. 4. The computed scattering angle distributions are broad with forward preference at low

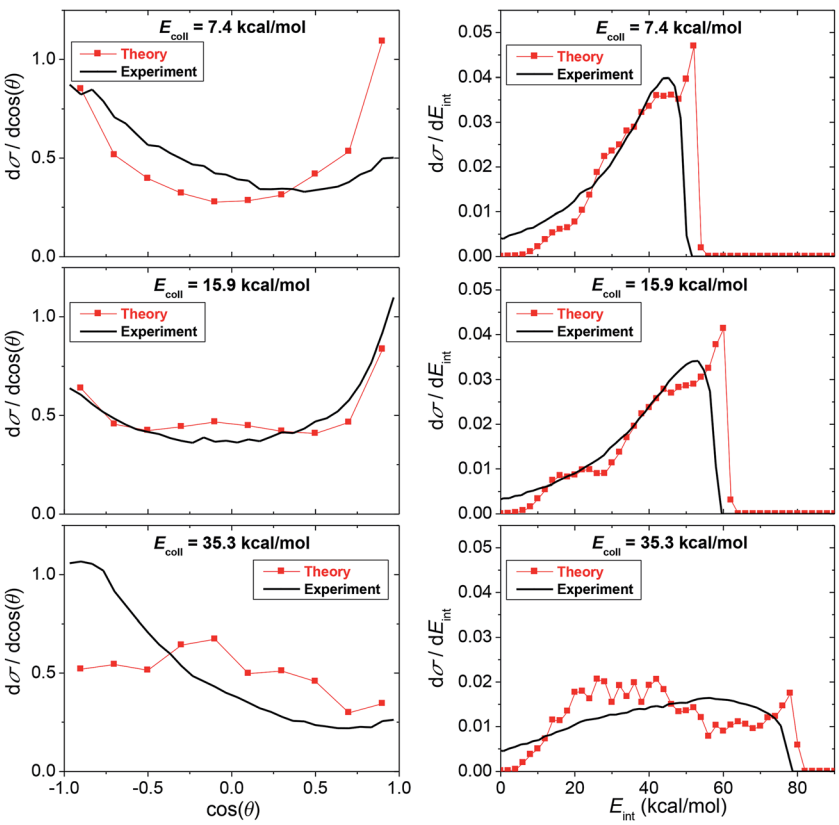

Fig. 4 Theoretical (this work) and experimental (ref. 12) normalized scattering angle and product internal energy distributions for the $F^- + CH_3I$ S_N2 reaction at different collision energies.

E_{coll} and slight backward dominance at larger E_{coll}. The broad nearly isotropic feature shows the dominance of the indirect reaction pathways in the $F^- + CH_3I$ S_N2 reaction. At low E_{coll} up to about 20 kcal mol^{-1} the CH_3F product internal energy distributions are hot peaking at the highest energies showing that most of the available energy transfers into product vibration and rotation which also supports the dominance of the indirect mechanisms. At a higher E_{coll} of 35.3 kcal mol^{-1}, the internal energy distributions are broader indicating mixed direct–indirect mechanisms. For the internal energy distributions theory and experiment are in good qualitative or semi-quantitative agreement as shown in Fig. 4. The finding that the maximum internal energy obtained from the simulation is higher by 1–2 kcal mol^{-1} than the experimental value is due to the fact that the analytical PES overestimates the exothermicity of the S_N2 channel by about 1 kcal mol^{-1}. The agreement between the computed and measured angular distributions is excellent at E_{coll} = 15.9 kcal mol^{-1}. At E_{coll} = 7.4 kcal mol^{-1}, theory shows more forward scattering than experiment, whereas at E_{coll} = 35.4 kcal mol^{-1} theory is more isotropic than the backward-scattered experiment. At this latter E_{coll}, the present computed angular distribution shows some agreement with the previous DFT/B91-1 direct dynamics result, which is also isotropic-like.[12] We should also note that the MP2 direct dynamics simulation starts to pick up the backward preference of the experiment.[34] However, it is clear that more work needs to be done to obtain definitive theoretical predictions for the angular distributions at high collision energies. Furthermore, it is interesting to note that the present angular distributions are much more isotropic and the internal energy distributions are significantly hotter than the corresponding distributions of the $F^- + CH_3Cl$ reaction. This supports our previous finding that the $F^- + CH_3Cl$ reaction is more direct than the analogous $F^- + CH_3I$ reaction showing a significant leaving group effect on the dynamics of S_N2 reactions.[7]

In order to further investigate the competition between direct and indirect mechanisms, we have determined the direct rebound, direct stripping, and indirect cross sections based on trajectory-integration-time *vs.* leaving-group-velocity correlation diagrams and scattering angle distributions as shown in more detail in Fig. S5.† The mechanism-specific reaction probabilities at different collision energies are given in Fig. S6.† As seen, the direct reactions proceed with rebound mechanism at small impact parameters and stripping trajectories occur at large b values. The overlaps between the rebound and stripping opacity functions are almost negligible. The indirect reaction probabilities usually decrease with increasing b. At the highest collision energies the indirect reactions vanish at the largest b values and almost solely stripping trajectories are found. The fractions of the rebound, stripping, and indirect cross sections as a function of the collision energy are shown in Fig. 5. At low E_{coll} up to about 20 kcal mol^{-1} the indirect mechanism dominates and at higher E_{coll} the direct pathways, especially *via* the rebound mechanism, become more significant. The computed direct rebound fractions of 17 and 49% at E_{coll} = 7.4 and 35.3 kcal mol^{-1}, respectively, are in excellent agreement with the corresponding experimental values of 20 and 52%.[12] At E_{coll} =

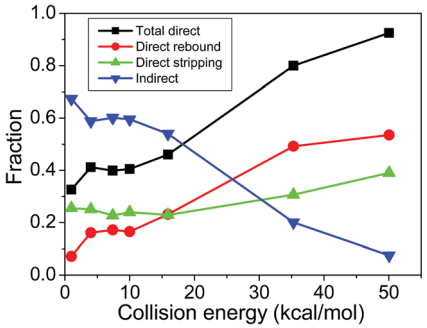

Fig. 5 Total direct (rebound + stripping), direct rebound, direct stripping, and indirect $F^- + CH_3I$ S_N2 cross section ratios as a function of collision energy.

35.3 kcal mol^{-1} the previous DFT/B91-1 direct dynamics simulation[34] gave cross section percentages of 29, 12, and 59 for the direct rebound, direct stripping, and indirect mechanisms, respectively, in disagreement with experiment and the present results of 49, 31, and 20%, respectively. Nevertheless, the agreement with the MP2 direct dynamics results[34] of 46, 43, and 11% is much better, which indicates that the DFT/B91-1 method may not give a reasonably accurate description of the PES at high energies. Although both experiment and the present theoretical results show that the direct rebound is the dominant mechanism of the $F^- + CH_3I$ reaction at high E_{coll}, the roughly 50% direct rebound fraction is significantly less than that (~80%) of the $F^- + CH_3Cl$ reaction, supporting our previous findings.[7]

Summary and conclusions

We have developed the first analytic global *ab initio* PES for the title reaction, which accurately describes both the S_N2 and proton-transfer channels. QCT simulations on the new PES reveal double-inversion trajectories for the $F^- + CH_3I$ reaction. Furthermore, the absolute cross sections of $F^- + CH_3I$ double inversion are found to be larger than those of the $F^- + CH_3Cl$ reaction. At low collision energies clearly the back-side attack dominates, at high energies the proton-transfer and S_N2 channels have similar reactivity. About 1% of the S_N2 trajectories occur *via* the double-inversion and front-side attack pathways. At low collision energies the double-inversion is the dominant retention mechanism, at higher energies the front-side attack pathway opens. The differential cross sections and product internal energy distributions of the $F^- + CH_3I$ S_N2 reaction usually show good agreement with experiment, although some differences can be observed, especially at high collision energies. Some of the results agree well with previous direct dynamics simulations, but there are also differences. The above findings clearly show that the title reaction is a challenging system and the standard single-reference electronic structure methods and effective core potentials used for the iodine atom may not give a good description at high potential energies. Nevertheless, the above-described dynamical results are just certainly the beginning of a fruitful research utilizing the analytical PES reported here for the $F^- + CH_3I$ reaction. We hope that the new PES will

open the door for several future dynamical investigations using quantum[37] as well as quasi-classical methods and considering vibrational and/or rotational mode specificity, isotope effects as well as different high-energy reaction channels.

Acknowledgements

G. C. thanks the Scientific Research Fund of Hungary (PD-111900) and the János Bolyai Research Scholarship of the Hungarian Academy of Sciences for financial support. We acknowledge the National Information Infrastructure Development Institute for awarding us access to resource based in Hungary at Debrecen and Szeged.

References

1 C. K. Ingold, *Structure and Mechanisms in Organic Chemistry*, Cornell Univ. Press, Ithaca, NY, 1953.
2 J. I. Brauman, *Science*, 2008, **319**, 168.
3 P. Manikandan, J. Zhang and W. L. Hase, *J. Phys. Chem. A*, 2012, **116**, 3061–3080.
4 J. Xie, R. Otto, J. Mikosch, J. Zhang, R. Wester and W. L. Hase, *Acc. Chem. Res.*, 2014, **47**, 2960–2969.
5 I. Szabó, A. G. Császár and G. Czakó, *Chem. Sci.*, 2013, **4**, 4362–4370.
6 I. Szabó and G. Czakó, *Nat. Commun.*, 2015, **6**, 5972.
7 M. Stei, E. Carrascosa, M. A. Kainz, A. H. Kelkar, J. Meyer, I. Szabó, G. Czakó and R. Wester, *Nat. Chem.*, 2016, **8**, 151–156.
8 J. Xie and W. L. Hase, *Science*, 2016, **352**, 32–33.
9 J. Mikosch, S. Trippel, C. Eichhorn, R. Otto, U. Lourderaj, J.-X. Zhang, W. L. Hase, M. Weidemüller and R. Wester, *Science*, 2008, **319**, 183–186.
10 P. Liu, D. Y. Wang and Y. Xu, *Phys. Chem. Chem. Phys.*, 2016, **18**, 31895–31903.
11 J. Zhang, J. Mikosch, S. Trippel, R. Otto, M. Weidemüller, R. Wester and W. L. Hase, *J. Phys. Chem. Lett.*, 2010, **1**, 2747–2752.
12 J. Mikosch, J. Zhang, S. Trippel, C. Eichhorn, R. Otto, R. Sun, W. A. de Jong, M. Weidemüller, W. L. Hase and R. Wester, *J. Am. Chem. Soc.*, 2013, **135**, 4250–4259.
13 J. Zhang, J. Xie and W. L. Hase, *J. Phys. Chem. A*, 2015, **119**, 12517–12525.
14 E. Carrascosa, T. Michaelsen, M. Stei, B. Bastian, J. Meyer, J. Mikosch and R. Wester, *J. Phys. Chem. A*, 2016, **120**, 4711–4719.
15 I. Szabó and G. Czakó, *J. Phys. Chem. A*, 2015, **119**, 3134–3140.
16 B. J. Braams and J. M. Bowman, *Int. Rev. Phys. Chem.*, 2009, **28**, 577–606.
17 J. M. Bowman, G. Czakó and B. Fu, *Phys. Chem. Chem. Phys.*, 2011, **13**, 8094–8111.
18 R. Conte, P. L. Houston and J. M. Bowman, *J. Chem. Phys.*, 2014, **140**, 151101.
19 R. Conte, C. Qu and J. M. Bowman, *J. Chem. Theory Comput.*, 2015, **11**, 1631–1638.
20 Y. Wang and J. M. Bowman, *Phys. Chem. Chem. Phys.*, 2016, **18**, 24057–24062.
21 T. B. Adler, G. Knizia and H.-J. Werner, *J. Chem. Phys.*, 2007, **127**, 221106.
22 T. H. Dunning Jr, *J. Chem. Phys.*, 1989, **90**, 1007–1023.
23 K. A. Peterson, D. Figgen, E. Goll, H. Stoll and M. Dolg, *J. Chem. Phys.*, 2003, **119**, 11113–11123.
24 G. Czakó and J. M. Bowman, *J. Phys. Chem. A*, 2014, **118**, 2839–2864.
25 H.-J. Werner, P. J. Knowles, G. Knizia, F. R. Manby, M. Schütz and others, *MOLPRO, version 2015.1*, *a package of ab initio programs*, see http://www.molpro.net.
26 W. L. Hase, *Encyclopedia of Computational Chemistry*, Wiley, New York, 1998, pp. 399–407.
27 R. Conte, P. L. Houston and J. M. Bowman, *J. Phys. Chem. A*, 2014, **118**, 7742–7757.
28 P. L. Houston, R. Conte and J. M. Bowman, *J. Phys. Chem. A*, 2014, **118**, 7758–7775.
29 R. Conte, P. L. Houston and J. M. Bowman, *J. Phys. Chem. A*, 2015, **119**, 12304–12317.
30 G. S. Hammond, *J. Am. Chem. Soc.*, 1955, **77**, 334–338.
31 G. Czakó and J. M. Bowman, *J. Chem. Phys.*, 2009, **131**, 244302.
32 L. Bonnet and J. Espinosa-García, *J. Chem. Phys.*, 2010, **133**, 164108.
33 G. Czakó, *J. Phys. Chem. A*, 2012, **116**, 7467–7473.
34 R. Sun, C. J. Davda, J. Zhang and W. L. Hase, *Phys. Chem. Chem. Phys.*, 2015, **17**, 2589–2597.
35 I. Szabó, H. Telekes and G. Czakó, *J. Chem. Phys.*, 2015, **142**, 244301.
36 I. Szabó and G. Czakó, *J. Chem. Phys.*, 2016, **145**, 134303.
37 Y. Wang, H. Song, I. Szabó, G. Czakó, H. Guo and M. Yang, *J. Phys. Chem. Lett.*, 2016, **7**, 3322–3327.

